

Investigation of interunit dispersion in 2D street canyons: A scaled outdoor experiment

Yuwei Dai^a, Cheuk Ming Mak^{a*}, Yong Zhang^b, Dongjin Cui^c, Jian Hang^b

^aDepartment of Building Services Engineering, The Hong Kong Polytechnic University, Hong Kong, China

^bSchool of Atmospheric Sciences, Guangdong Province Key Laboratory for Climate Change and Natural Disaster Studies, Sun Yat-sen University, Guangzhou, P.R. China 510275

^cSchool of Architecture & Urban Planning, Shenzhen University, Shenzhen 518060, P. R. China

*Corresponding author: Cheuk Ming Mak
Email: cheuk-ming.mak@polyu.edu.hk

Abstract

Interunit dispersion problems have been studied previously mainly through on-site measurements, wind tunnel tests, and CFD simulations. In this study, a scaled outdoor experiment was conducted to examine the interunit dispersion characteristics in consecutive two-dimensional street canyons. Tracer gas (CO_2) was continuously released to simulate the pollutant dispersion routes between the rooms in street canyons. The wind velocity, wind direction, air temperature, and tracer gas concentrations were monitored simultaneously. Two important parameters, the air exchange rate and reentry ratio, were analyzed to reveal the ventilation performance and interunit dispersion of the rooms in the street canyons. Based on the real-time weather conditions, it was found that the ventilation performance of the source room varied according to the room location. The air exchange rate distribution of the leeward-side room was more stable than that of the windward side. The tracer gas was mainly transported in the vortex direction inside the street canyon, and the highest reentry ratio was observed at the room nearest to the source room along the transportation route. In addition, under real weather conditions, the rooms in the street canyon have a high probability of experiencing a high reentry ratio based on the maximum reentry ratio of each room. This study provides authentic airflow and pollutant dispersion information in the street canyons in an urban environment. The dataset of this experiment can be used to validate further numerical simulations.

Keywords: scaled outdoor experiment, street canyon, tracer gas method, ventilation rate, interunit dispersion.

1. Introduction

Indoor air quality (IAQ) has a significant impact on human health because people spend most of their time indoors [1, 2]. A poor IAQ, caused by the concentrations of particulate matter and gaseous pollutants in the air, may lead to harmful consequences to human health. Various pollutants, such as traffic exhaust, dust, pollen, airborne viruses, and toxic and odorous emissions, may enter indoor areas [3]. Recently, a special mode of pollutant transmission, known as interunit dispersion, has gained popularity. Interunit dispersion illustrates the cross-transmission between apartment units within the same multistory building. This airborne transmission mode is highly risky because of the relatively short dispersion distances and transportation time as compared to other modes like pollutants from special dense sources and traffic exhausts [4].

There are two main circumstances that need to be considered in a densely populated city. First, during mild seasons, people may adopt natural ventilation as their main ventilation strategy [5-8], which may increase the incursion of outdoor pollutants to indoor areas through windows [9]. Second, outbreaks of acutely infectious diseases or even the ordinary flu season [10] may result in airborne viruses or biological aerosols in the airflow, which poses a great threat to public health. Therefore, a more detailed understanding of the mechanism and features of interunit dispersion in the urban environment, is necessary.

Interunit dispersion was identified during the outbreak of Severe Acute Respiratory Syndrome (SARS) in Hong Kong in 2003 [11, 12]. Since then, a substantial number [12-18] of studies have continued to investigate the pollutant dispersion among units in the same building and the airflow field around the built environment. Recently, Mao et al. [13] summarized the existing studies by targeting the interunit transmission and dispersion problems. Several methods, such as on-site measurements, wind tunnel experiments, and Computational Fluid Dynamics (CFD) simulations, have been adopted to investigate the coupled indoor and outdoor airflow and pollutant dispersion in a naturally ventilated environment.

Niu and Tung [14] conducted on-site measurements to investigate the vertical interunit dispersion mechanism and proposed a possible pollutant transmission route in a residential building. Using the tracer gas technique, they found that the reentry ratio of the exhaust air from a lower unit to the immediate upper unit can reach 7%. Their measurements were conducted under real atmospheric conditions that could represent completely authentic wind and weather situations. However, the results of this study were limited to upward transportation between two vertically adjacent units. The pollutants released from the lower unit may also enter other upper units [15]. In addition, the on-site measurements were accompanied by various uncertainties such as the irregular geometries of the residential buildings.

Later, a number of wind tunnel experiments [16-19] were carried out targeting the interunit transmission issue. These wind tunnel experiments only considered wind-dominated effects and focused on multistory residential buildings with various wind directions and source locations. The results revealed that the pollutants released from a unit may spread both vertically and horizontally in the same building.

CFD simulations were also commonly used to investigate the interunit transmission. A series of numerical studies were conducted to further understand the influential factors of interunit dispersion, including the effects of buoyancy-dominated forces [15, 20-22], balconies [10, 23, 24], surrounding interfering buildings [25, 26], and heated walls [27]. Different turbulence models were considered in the airflow and dispersion simulations, including a mean process with an advanced Reynolds-Averaged Navier-Stokes (RANS) model [10, 23, 25, 26] and transient process with an Large-Eddy Simulation (LES) model [24, 28]. However, the wind tunnel experiments and CFD simulations were based on assumed atmospheric boundary conditions, which do not consider realistic factors of the urban environment. Considering the complexity of urban environments, more experimental studies are required to investigate the issues pertaining to interunit dispersion.

Recently, researchers have adopted scaled outdoor experiments as effective alternatives to on-site measurement, wind tunnel experiments, and CFD simulations, to investigate the airflow field and pollutant dispersion in the urban environment. Yee and Biltoft [29] investigated the characteristics of a pollutant dispersion through a 10×12 array of building-like obstacles in the scaled outdoor Mock Urban Setting Test facility in Utah, USA. Later, Dallman et al. [30] used two rows of shipping containers to construct a mock street canyon to investigate nonuniform wind and thermal effects in a two-dimensional (2D) street canyon.

More recently, Comprehensive Outdoor Scale Model experiments have been conducted in Japan. The model was built using a regular array of large concrete cubes on a concrete base to keep the thermal inertial similarity with the real urban environment [31-35]. Scaled outdoor experiments were performed to investigate problems involving the turbulent flow in an urban

canopy layer, the surface energy balance, and pollutant dispersion in an urban environment. The results of these studies revealed that an outdoor scale model can be regarded as an idealized scaled-down city without human interference and with a diversity of building geometries. This allows for detailed measurements of urban environments.

Compared to on-site measurements, scaled outdoor experiments can reduce the uncertainties associated with different surrounding geometries and materials of pollutant source areas [32]. Compared to wind tunnel experiments and CFD simulations, scaled outdoor experiments can provide authentic information of the wind and weather conditions in an urban environment. In addition, the scaled models can mitigate some ambiguities caused by wind tunnel and numerical simulations such as low turbulence intensities in the free stream of wind tunnel experiments and wall function settings in CFD simulations [34].

In order to further investigate the interunit dispersion problem, this study conducted an outdoor experiment in 2D street canyons on the Scaled Outdoor Model Urban Climate and Health (SOMUCH) field at Sun Yat-sen University. The tracer gas method using carbon dioxide (CO_2) was adopted to simulate the pollutant dispersion process in the street canyons. The study also intended to provide a complementary method between the on-site measurements and numerical simulations of the interunit dispersion in street canyons and provide authentic airflow and pollutant dispersion information under an urban environment. In addition, the dataset of this experiment can offer validation of further numerical simulations. Section 2 introduces the experiment setting and analysis methodology. Detailed results and discussions are presented in Section 3. Section 4 discusses the limitations of this study, and section 5 summarizes and concludes the study.

2. Methodology

2.1 Experiment settings and instrumentation

The SOMUCH experimental field is located on the southern side of Guangzhou, China ($23^{\circ}01'N$, $113^{\circ}24'E$). The field consists of a $57\text{ m} \times 57.5\text{ m}$ concrete foundation and around 2000 building models to simulate an idealized urban environment. The dimension of each building model is length \times width \times height = $0.5\text{ m} \times 0.5\text{ m} \times 1.2\text{ m}$. The building models are hollow concrete cuboids painted dark gray and have a wall thickness of 1.5 cm . The whole north/south street canyon field is $44.4\text{ m} \times 12\text{ m}$, the street canyon deviates by around 30° from the northern direction, as shown in Fig. 1. The street canyon consists of 33 arrays of cuboids with 4 kinds of aspect ratios (height to width) of 1: 1, 2: 1, 3: 1, and 6: 1. The length of each street canyon is 12 m . This study chose a 1: 1 street canyon as the target area, as shown in Fig. 1. The measurements lasted from June 7 to 10, 2019; on each day, the measurements lasted around from 9 am to 10 pm.

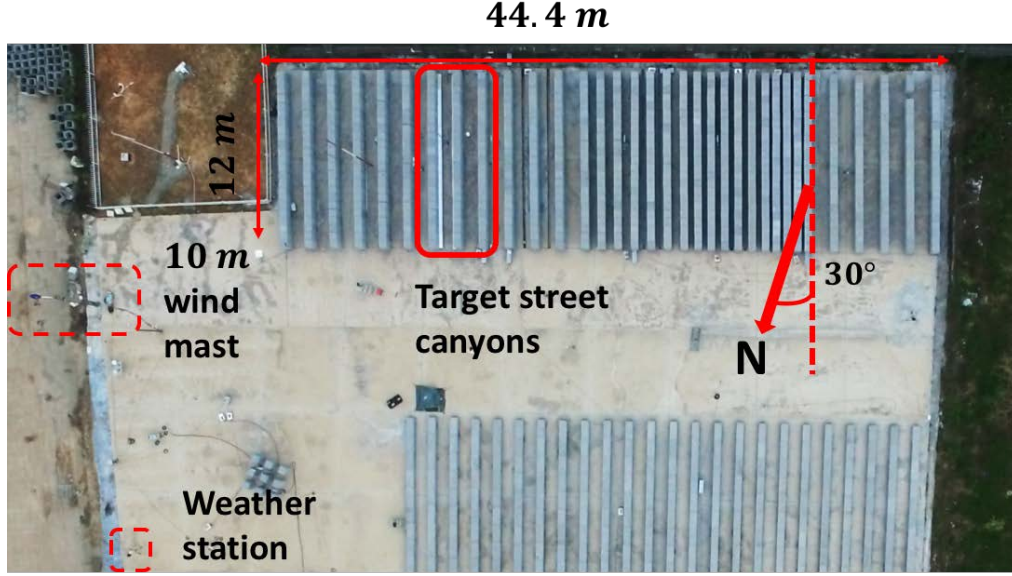


Fig. 1 Overview of experiment field.

In order to investigate the interunit dispersion, three acrylic models were customized. The customized models had the same dimensions as the concrete models but had four floors with two opposite rooms on each floor, and each room had an opening with a height and width of 0.1 m and 0.2 m , respectively. The dimensions of the customized and concrete models are shown in Fig. 2. Carbon dioxide (CO_2) was adopted as the tracer gas in this experiment because of the availability of multiple measuring points (24 points at same time) and short response time (1 s). In order to avoid solar radiation and mitigate the greenhouse effect, each customized model was covered with tinfoil. Three acrylic models were placed separately in the middle of three adjacent building arrays in the 1:1 street canyons, as shown in Fig. 2(c).

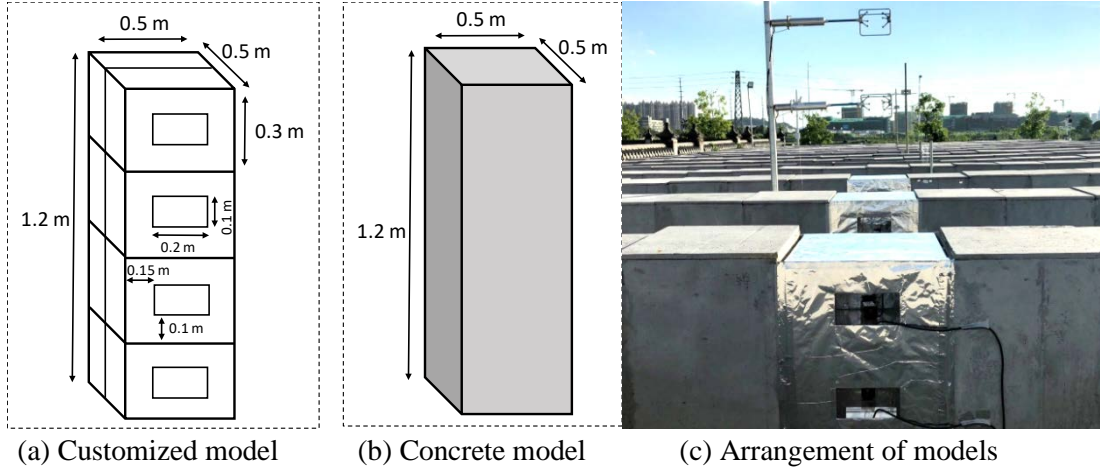


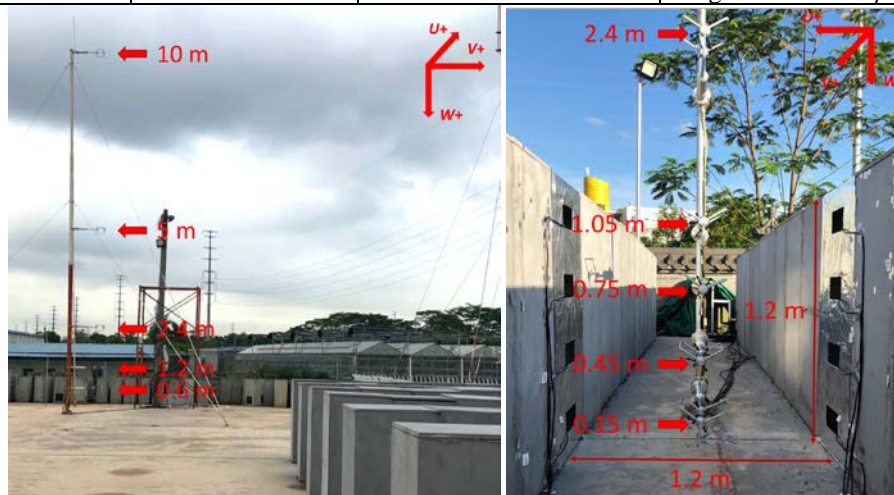
Fig. 2 Dimensions and arrangement of customized and concrete models.

Wind velocity, wind direction, air temperature, and CO_2 concentrations were the parameters that were measured during this study. Table 1 lists the measured parameters, equipment, and their accuracies. Two wind masts, each equipped with five ultrasonic anemometers, were planted on the field. The wind mast used to measure the far-field incoming flow velocities had a height of 10 m , the position is marked in Fig. 1. The five ultrasonic anemometers were placed at 0.6 , 1.2 , 2.4 , 5 and 10 m , as shown in Fig. 3(a). Another wind mast was used to measure the wind velocities in the street canyon. The heights of the five

ultrasonic anemometers placed on this mast were 0.15, 0.45, 0.75, 1.05, and 2.4 m. The heights of the lower four ultrasonic anemometers were set at the middle of the opening on each floor in the street canyon, as shown in Fig. 3(b). Twenty-four CO_2 sensors were placed near the opening of each room to measure the indoor concentration and inlet of the CO_2 sensor facing the opening of the room, as shown in Fig. 4(a). CO_2 , which was used as the tracer gas, was transported into the source room via a long tube with a diameter of 8 mm from a compressed gas cylinder. A customized plastic ball was installed in the middle of the source room and at the end of the tube to diminish the injection velocity. The diameter of the plastic ball was 30 mm. Six uniformly arranged holes with diameters of 5 mm were drilled in the plastic ball for the multidirectional release of the tracer gas, as shown in Fig. 4(b) and (c).

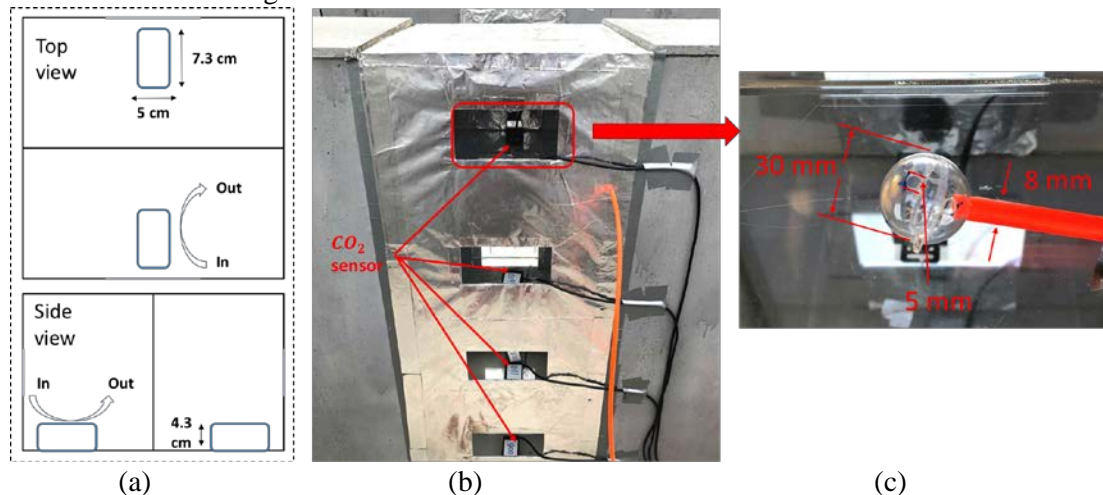
Table 1 Summary of parameters measured and equipment used.

Parameters	Equipment	Manufacturing company	Accuracies
Wind speed	3D ultrasonic anemometer	Gill Instruments Limited.	1.5% in a range of 0 – 50 m/s
Indoor/outdoor air temperature	K type fine-wire thermocouple ($\Phi 0.127$ mm)	Agilent Technologies Inc. (Data logger)	0.4% in a range of $-200 - 260^\circ\text{C}$
CO_2 concentration	CO_2 sensor	HR International Co.	± 40 ppm in a range of 400 – 10000 ppm
Background air temperature and wind speed	Automatic weather station	RainWise Inc.	$\pm 0.25^\circ\text{C}$ in range of $-54 - 74^\circ\text{C}$, $\pm 2\%$ in range of 0 – 67 m/s



(a) 10-m mast (b) 2.4-m mast

Fig. 3 Positions of two wind masts for wind velocities.



(a)

(b)

(c)

Fig. 4 (a) Schematic view of positions of CO_2 sensors in each room, In: inlet of the CO_2 sensors, Out: outlet of the CO_2 sensors. (b) and (c): Setup for tracer gas release.

The background wind velocities and directions were measured using a RainWise automatic weather station placed at a height of 2.4 m (2 times of the model height) [36], the position is marked in Fig. 1. Fig. 5 presents the wind rose maps and velocity frequencies during the measurement periods on June 8 and 9, 2019. The prevailing wind directions were mostly between 225° – 270° , especially on June 9, 2019. The incoming wind was approximately perpendicular to the street canyon. During the measurement, the air temperature of the scaled outdoor field varied from 26.9°C – 34.9°C .

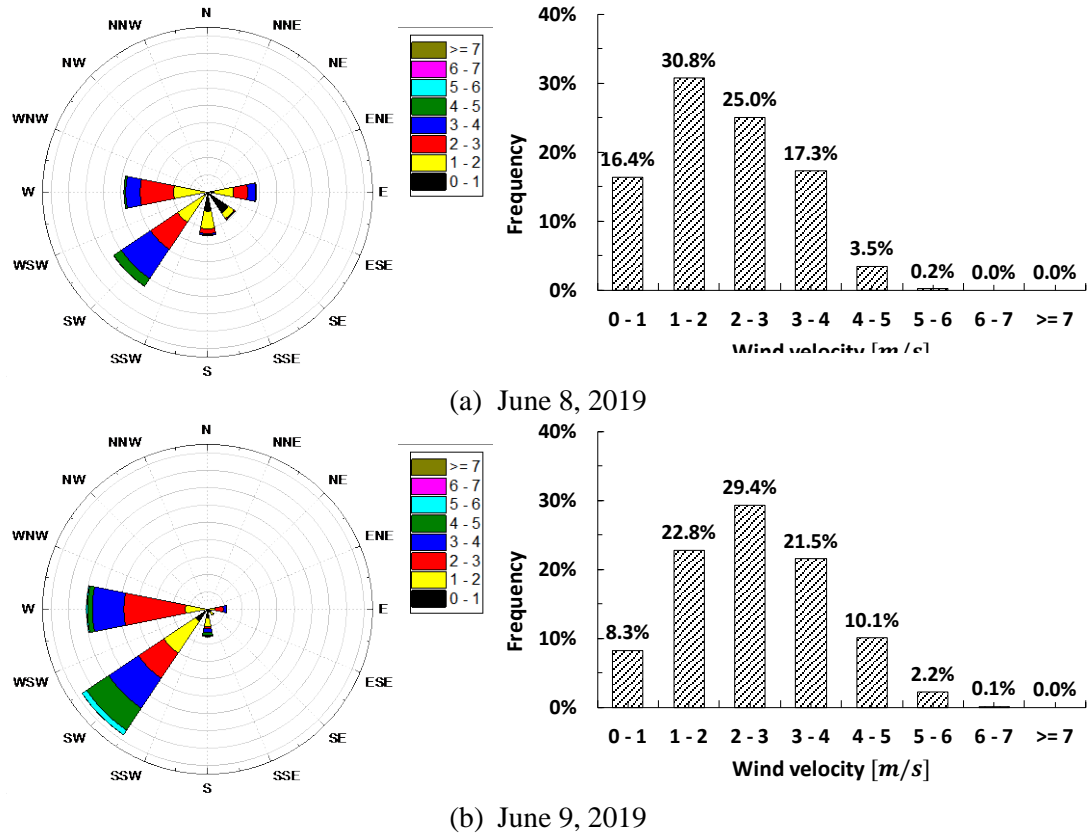


Fig. 5 Wind rose maps and velocity frequencies during measurements.

2.2 Experiment design

As shown in Fig. 6, building B was set as the source building. In Fig. 6, W represents the windward side, and L represents the leeward side. During the tests, each room in building B was set as the source room, and the tracer gas was released continuously for around 30 min. The sampling frequency was 1 Hz and the output results were averaged for 1 s. The concentration of the source gas was 10^5 ppm , and the flow rate was 1.5 L/min . All instruments were sampled simultaneously for the wind velocity, wind direction, air temperature, and CO_2 concentrations in each room. After completing one test, the gas releasing tube was pulled out. The next test was not initiated until the CO_2 concentration in the former source room declined to its initial status. Each room in Building B as a source location was a single test, a total of eight tests (eight source rooms) were included as a full round of tests. During the entire experiment, a total of three full rounds of tests were conducted from June 8 to 10, 2019. Table 2 lists the information of three rounds of tests, wind direction and velocity were measured by weather station. Noted that, the tracer gas of three tests (Round 3 BL1, BL3 and BL4) was released for around 20 min.

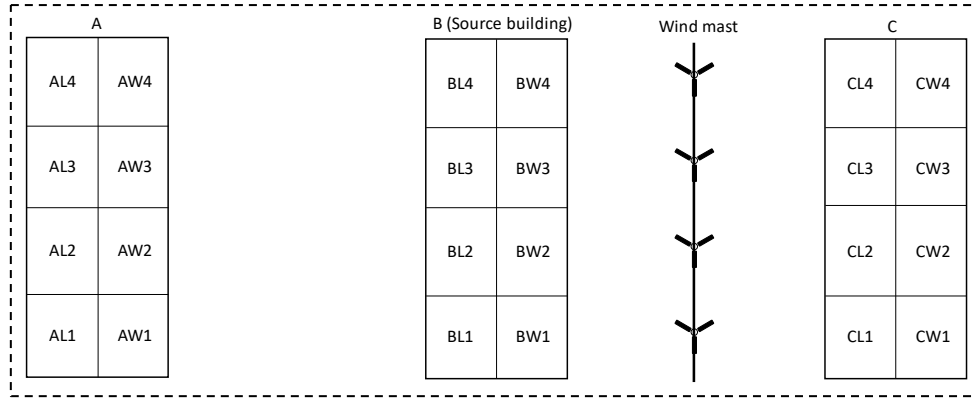


Fig. 6 Schematic view of source room.

Table 2 Summary of the three rounds of tests from June 8 to 10, 2019.

	Source Room	Date	Time period	Wind direction [°]	Wind velocity [m/s]
Round 1	BL1	June 8	09:46:00-10:16:00	218.8	2.14
	BL2	June 8	10:32:00-11:02:00	228.9	3.13
	BL3	June 8	11:23:00-11:53:00	233.5	3.21
	BL4	June 8	12:12:00-12:42:00	238.9	3.26
	BW1	June 8	18:57:00-19:28:00	133.8	2.59
	BW2	June 8	18:10:00-18:40:00	192.7	2.41
	BW3	June 8	15:53:00-16:23:00	193.3	1.85
	BW4	June 8	17:18:00-17:48:00	193.7	2.79
Round 2	BL1	June 9	14:16:00-14:46:00	235.5	4.15
	BL2	June 9	15:11:00-15:41:00	244.4	2.73
	BL3	June 9	16:13:00-16:43:00	231.4	2.68
	BL4	June 9	17:09:00-17:39:00	250.6	3.01
	BW1	June 9	10:40:00-11:10:00	233.1	4.12
	BW2	June 9	11:32:00-12:02:00	231.9	3.42
	BW3	June 9	12:27:00-12:57:00	229.1	4.14
	BW4	June 9	13:19:00-13:49:00	233.4	3.55
Round 3	BL1	June 9	19:06:00-19:26:00	230.5	2.87
	BL2	June 8	21:19:00-21:49:00	196.7	1.26
	BL3	June 8	20:32:00-20:54:00	187.2	1.51
	BL4	June 8	19:49:00-20:09:00	219.9	1.94
	BW1	June 10	12:19:00-12:49:00	228.4	3.62
	BW2	June 10	11:35:00-12:05:00	228.0	3.19
	BW3	June 10	10:51:00-11:21:00	236.0	3.45
	BW4	June 10	09:45:00-10:15:00	228.2	3.19

2.3 Data analysis method

The tracer gas method has been widely used to determine the air exchange rates in buildings [37, 38]. Assuming a steady flow and well-mixed tracer gas, the calculation of the ventilation rate of the source room based on the principle of mass conservation can be achieved by the following equation:

$$V \frac{dC_{in}}{dt} = Q(C_{out} - C_{in}) + S \quad (1)$$

where C_{in} is the indoor CO_2 concentration (ppm), C_{out} is the CO_2 concentration in ambient fresh air (ppm), V is the volume of the room (m^3), Q is the flow rate of the air (m^3/s), and S is the emission rate of the tracer gas source (m^3/s). The ventilation rate can be converted to air exchange per hour (ACH), based on equation (1), as

$$ACH = \frac{Q}{V} = \frac{\frac{dC_{in}}{dt} - \frac{S}{V}}{C_{out} - C_{in}} \quad (2)$$

During a period of $\Delta t = t_{i+1} - t_i$ (h), the ventilation rate of a room can be expressed as

$$ACH = \frac{S\Delta t - (C_{in,t_{i+1}} - C_{in,t_i})V}{(C_{in,t_i} - C_{out})\Delta t V} \quad (3)$$

where C_{in,t_i} and $C_{in,t_{i+1}}$ represent the tracer gas concentration of the room at times t_i and t_{i+1} , respectively.

The reentry ratio is another indicator that was used to assess tracer gas transportation between the source and other rooms. In this study, the reentry ratio was defined as the fraction of the tracer gas from the source room that reenters another room during each time interval. This can be calculated by

$$R_k = \frac{(C_{i,t_i} - C_{out})V_i}{S\Delta t - (C_{j,t_{i+1}} - C_{j,t_i})V_j} \quad (4)$$

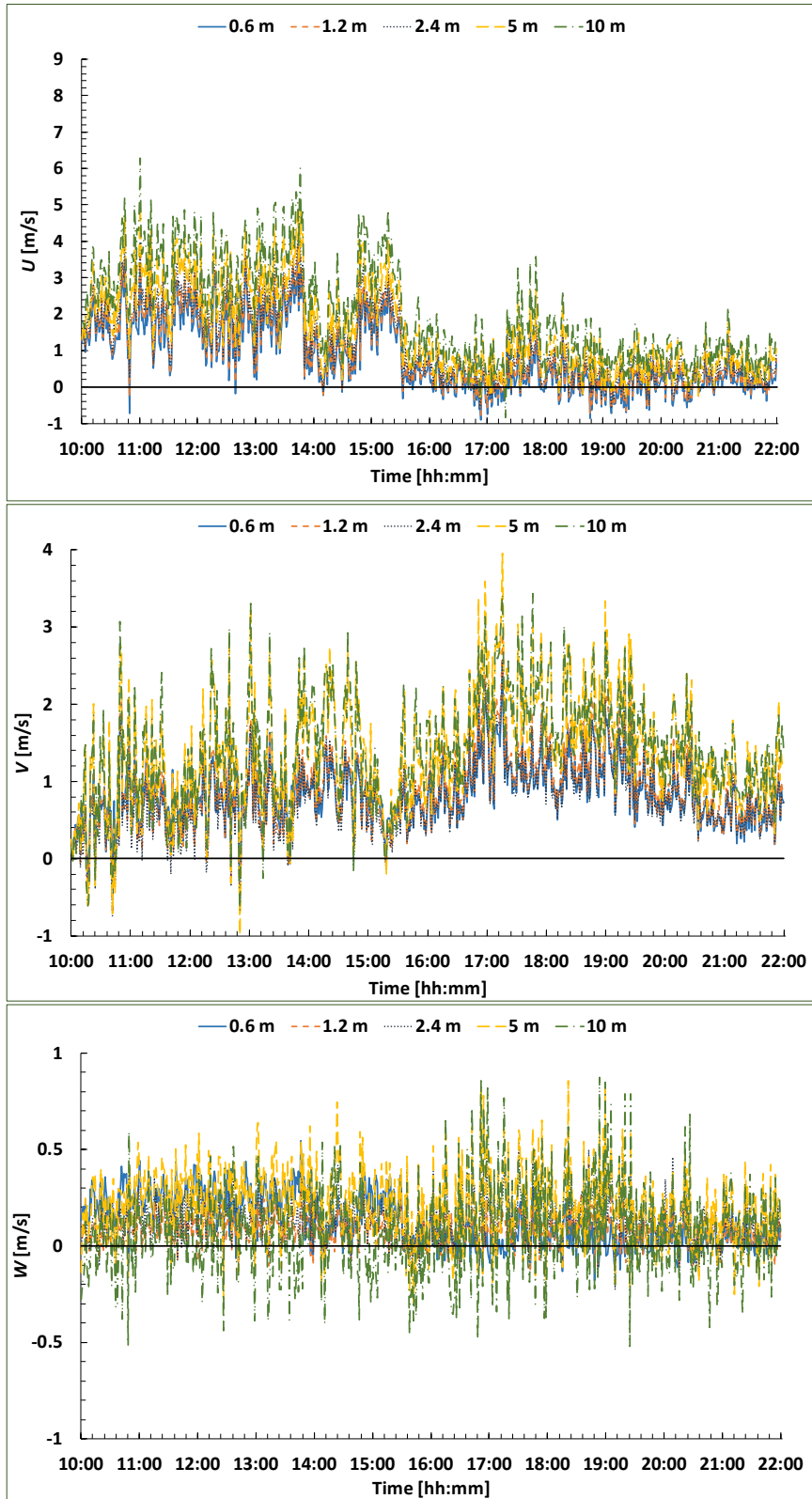
where C_{i,t_i} is the measured concentration of the tracer gas in the reentered room at time t_i , C_{j,t_i} is the concentration of the source room at time t_i , S is the concentration of the source tracer gas, Δt is the time interval, and V_i and V_j are the volumes of the source and reentered rooms, respectively.

3. Results and discussions

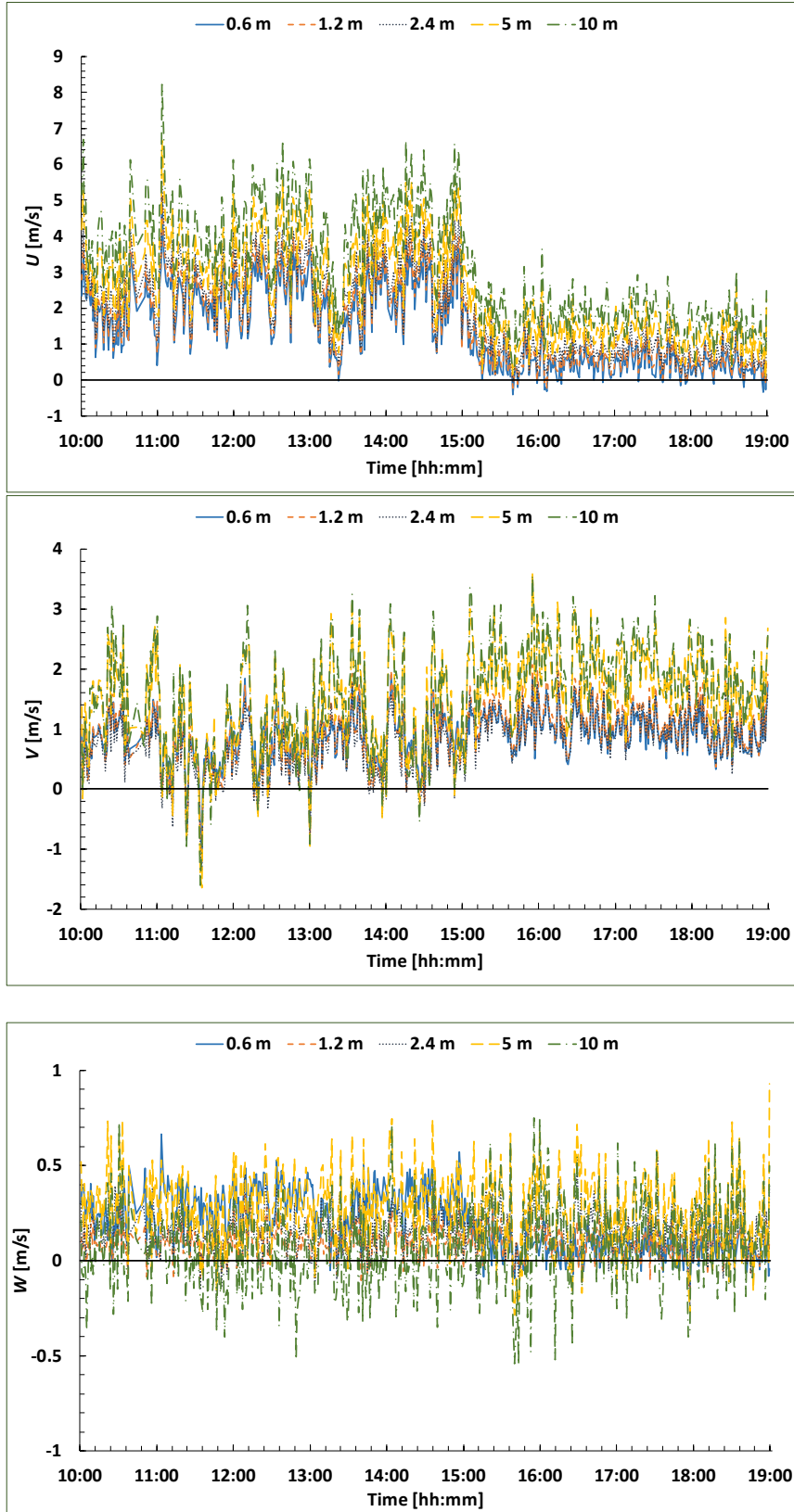
3.1 Monitored weather conditions

3.1.1 Wind conditions during test period

Fig. 7 shows the incoming wind during two test days, monitored by the 10-m wind mast. Noted that, the data from 10:43:58 to 10:49:56 on June 9 are missing because of an equipment malfunction. The wind velocities are presented as vector components in which $U +$ is the southern direction, $V +$ is the eastern direction, and $W +$ is the downward direction, a coordinate system is shown in Fig. 3. Compared to the data from June 8, on June 9, the vector component U stayed positive for a majority of the test time, which indicates that the incoming wind was very stable and barely flowed in the reverse direction. Therefore, for convenience in the analysis, the test cases from June 9, 2019, are adopted for most of the following discussion.



(a) June 8



(b) June 9

Fig. 7 Wind profiles during test periods on June 8 and 9, 2019, by a 10-m wind mast.

As an obvious reduction was observed in component U , as shown in Fig. 7, the wind profile is separated into two phases by the time of 15:00:00 to better fit the velocity curve. Fig. 8 shows the average wind components and fitted U profiles of the two phases on June 8 and 9, 2019. The standard deviation of the measured errors for the wind velocity were within 5%

which confirmed the error bar is 5% in Fig. 8. The power law is adopted to construct the wind profile equations and can be expressed by

$$\frac{U}{U_H} = \left(\frac{Z}{Z_H} \right)^\alpha \quad (5)$$

where U is the wind velocity at height Z , U_H is the referenced velocity at the street canyon height, Z_H is the street canyon height, and α is the empirical coefficient. In this experiment, the incoming wind profiles were obtained by fitting U , on June 8, $U_H = 1.82 \text{ m/s}$, $Z_H = 1.2 \text{ m}$, $\alpha = 0.255$ in phase I and $U_H = 0.39 \text{ m/s}$, $Z_H = 1.2 \text{ m}$, $\alpha = 0.525$ in phase II, as shown in Fig. 8(a) and (b); on June 9, $U_H = 2.46 \text{ m/s}$, $Z_H = 1.2 \text{ m}$, $\alpha = 0.245$ in phase I and $U_H = 0.63 \text{ m/s}$, $Z_H = 1.2 \text{ m}$, $\alpha = 0.495$ in phase II, as shown in Fig. 8(c) and (d), in the power law.

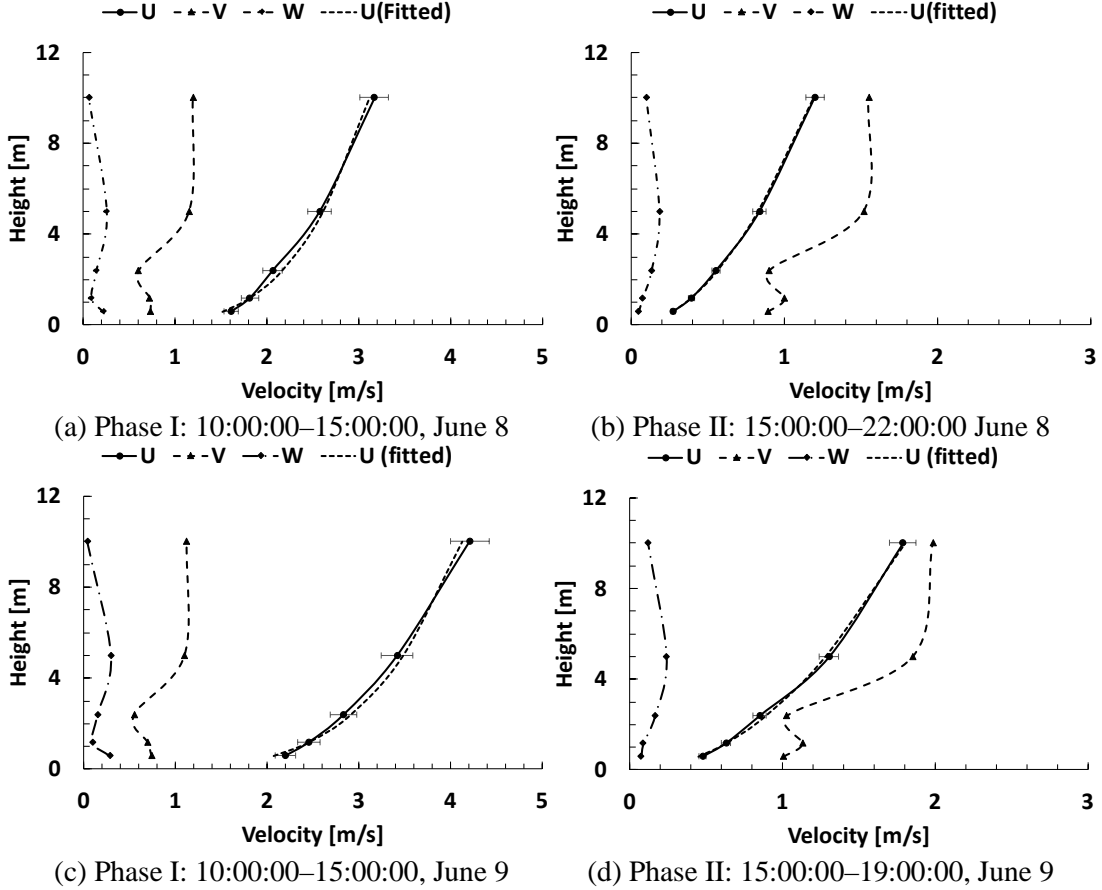


Fig. 8 Average wind components and fitted U profiles of June 8 and 9.

Fig. 9 shows the U component by the wind mast in the middle of the street canyon during the test periods on June 9. Noted that the data of 2.4 m after 14:33:30 are missing because of an equipment malfunction. Several observations can be made from the wind profile. First, two opposite airflow directions existed in the middle of the street canyon. The wind flow at heights of 0.75 m and 1.05 m followed the incoming wind direction for most of the measuring time except at a few points, while the wind flow at heights of 0.15 m and 0.45 m was in the reverse direction. This reveals a counterclockwise-rotating vortex in the street canyon produced by the freestream flow. This result is consistent with the airflow field in the 1:1 street canyon from previous research [36, 39, 40], which further implies the good stability of the wind condition on June 9, 2019.

Second, in the lower part of the street canyon, the wind velocity at a height of 0.15 m was higher than that at 0.45 m . Similarly, the wind velocity at a height of 1.05 m was higher than that at 0.75 m in the upper part of the street canyon. The relatively low wind velocity in the central part of the street canyon may not facilitate the dilution of the tracer gas. In addition,

after the time of 15:00:00, there was a significant reduction in the absolute value of the wind velocities ($|U|$) at the measuring points in the street canyon, which was consistent with the wind profile measured by the 10-m wind mast.

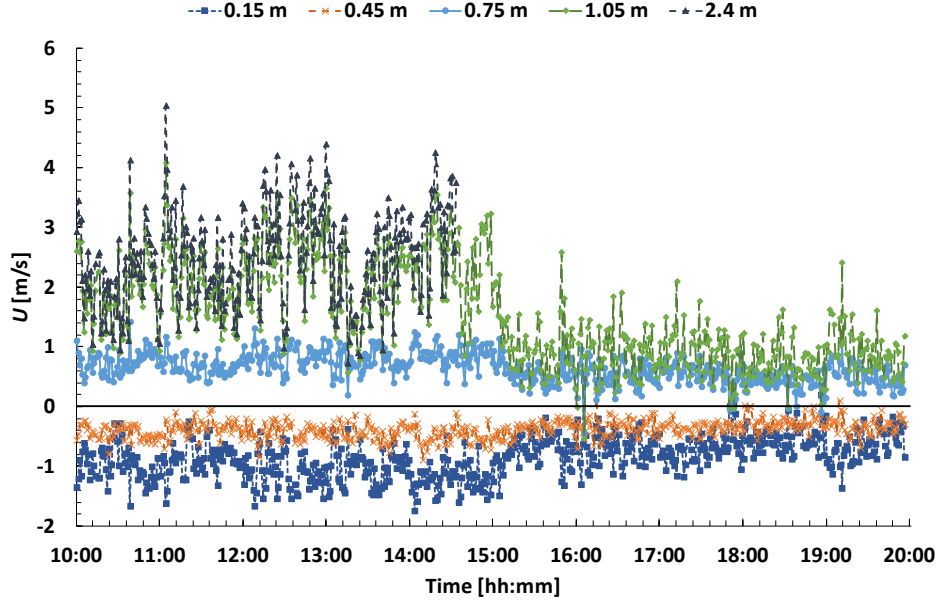


Fig. 9 Wind velocities during test periods on June 9, 2019, by 2.4-m wind mast in street canyon.

3.1.2 Thermal conditions during test period

Indoor and outdoor air temperatures were monitored during the test period. To measure the indoor air temperature, eight thermocouples were set in each room on the windward side of building B and leeward side of building C. As this was a consecutive street canyon with the same aspect ratio (1:1), the windward and leeward side rooms of the street canyon were considered identical with regard to the air temperature. To measure the outdoor air temperature, four thermocouples were set on the wind mast in the street canyon at heights of 0.15, 0.45, 0.75, and 1.05 m.

Table 3 lists the indoor and outdoor temperature differences during the test period. ΔT is calculated using $\Delta T = T_{in,z} - T_{out,z}$, where $T_{in,z}$ represents the indoor air temperature on each floor, and $T_{out,z}$ represents the outdoor air temperature at the corresponding height. Because of the solar heat gain, the indoor temperature was generally higher than the outdoor temperature. In addition, owing to the direction of the sun, the indoor temperatures of the rooms on the leeward side of building C were even higher. The maximum temperature difference occurred in room CL4, where the temperature difference reached 5.5°C.

Table 3 Indoor and outdoor temperature difference.

ΔT (K)	BW1	BW2	BW3	BW4	CL1	CL2	CL3	CL4
Mean	0.5	1.7	1.0	1.0	0.9	1.6	2.5	3.8
Max	1.9	3.8	2.9	2.3	1.9	2.8	3.8	5.5
Min	-1.5	-1.3	-0.7	-0.4	0.0	0.2	0.9	1.4

To characterize the buoyancy and wind effect in the street canyon, the Richardson number (Ri) is adopted [41]:

$$Ri = \frac{g\beta\Delta TH}{(U_H)^2} \quad (6)$$

where β is the thermal expansion coefficient and g is the gravitational acceleration (m^2/s). Considering the two wind phases described in section 3.1.1, during the tests of Round 2 on June

9, Ri varied from 0.0063 (phase I) to 0.53 (phase II). Typically, when $Ri < 0.1$, the buoyancy effect is negligible, which means during phase I, the influence of the thermal effect was overwhelmed by the wind effect in the street canyon. During phase II, $0.1 < Ri < 10$, which means the buoyancy effect was combined with wind effect in the street canyon.

Concerning the buoyancy effect during phase II, the average ventilation rate due to the temperature difference can be estimated by the following equation [42]:

$$ACH_B = \frac{C_d A_w \sqrt{\frac{gh\Delta T}{T_{in} z}}}{V} \quad (7)$$

where C_d is a discharge coefficient, 0.207 for a scaled model [43], A_w is the window area (m^2) and h is the opening height (m). During phase II on June 9, three tests were included, which were BL2, BL3 and BL4. Table 4 lists the estimated ventilation rates of the phase II tests due to the indoor and outdoor temperature differences.

Table 4 Ventilation rates of phase II tests with buoyancy effect.

h^{-1}	BL2	BL3	BL4
ACH_B	0.53	0.66	0.82

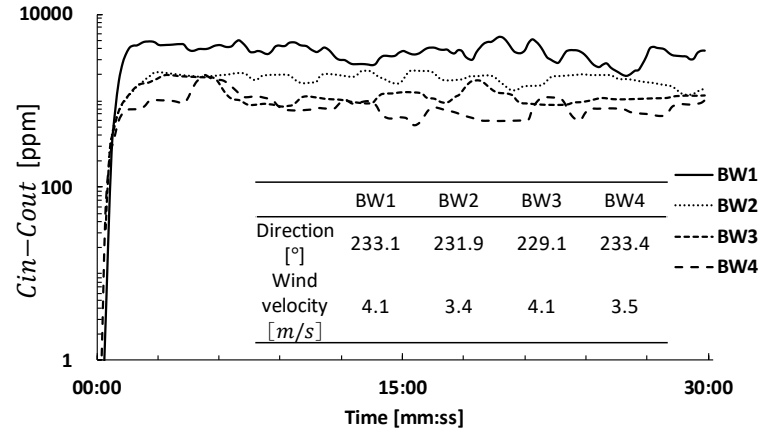
Since the buoyancy effect was not the focus of the current study, it was not analyzed as an influencing parameter on the tracer gas dispersion. This paper mainly analyzes the wind effect on the tracer gas dispersion, the combined buoyancy and wind effect on the tracer gas dispersion will be studied in the future.

3.2 Ventilation rate of source rooms

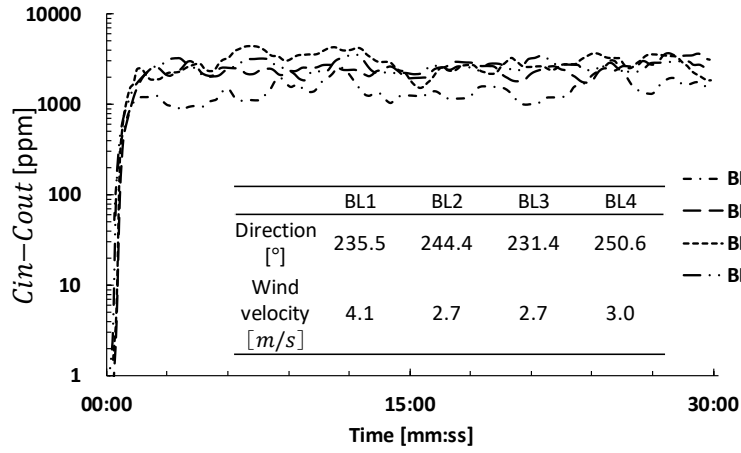
The wind directions on June 9, 2019, were more stable than those on June 8, as shown in Fig. 5 and 7. Therefore, in this section, the data from Round 2 on June 9, 2019, were acquired to analyze the ventilation rate of the source rooms. During each test, the CO_2 concentration of the source room was measured. Fig. 10 shows the active CO_2 concentration of the source room during the gas releasing period, and the average wind directions and velocities at a reference height of 2.4 m for each test. The CO_2 concentration of each room is presented in a logarithmic scale, and the background CO_2 concentration (C_{out}) is subtracted. At the beginning of the gas releasing period, the monitored CO_2 concentration in each room increased very quickly and then fluctuated drastically owing to the wind effect.

Two observations can be made based on the comparisons of the different tests. First, regarding the perpendicular direction to the street canyon (240°), the average wind directions of all tests varied within 10.9° , which implied that the wind direction may not be the main factor that caused the highly fluctuated CO_2 concentration in each room.

Second, when the source room was located on the windward side (BW1 to BW4), the average CO_2 concentration decreased when the height of the room increased. This may be attributed that, on the windward side, the near-wall airflow perpendicular to the facade was stronger with the increased room height, which indicated larger inflows and outflows through the openings located on the top part of the street canyon. However, this observation was not obvious when the source room was located on the leeward side.



(a) Source room located on windward side



(b) Source room located on leeward side

Fig. 10 CO_2 concentration of each source room during gas releasing process for 30 min, and average wind direction and velocity during each test.

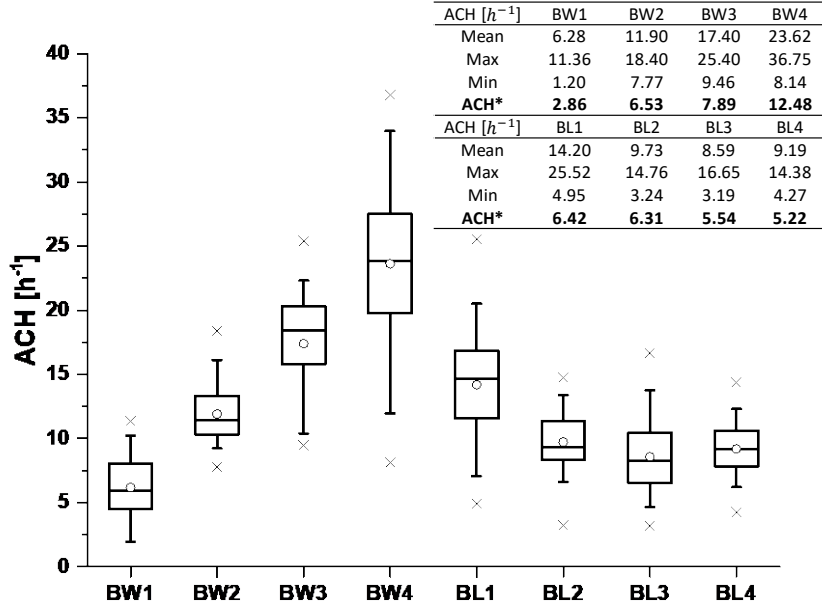


Fig. 11 Box charts of ACH values of each test.

Fig. 11 presents box charts of the ACH values calculated from CO_2 concentration data during each test by equation (3). The data from initial 60s were excluded. The box edges represent the 25th and 75th percentiles. A line in the box represents the 50th percentiles of a data group, and the whiskers represent the 5th and 95th percentiles. The symbol (○) indicates

the mean value of each data group, and the symbol (×) at the top and bottom of the whiskers indicates the maximum and minimum values. ACH^* is the dimensionless ventilation rate calculated by $ACH^* = \frac{ACH}{\bar{U}} \cdot \frac{V}{A_w}$ [27], where \bar{U} represents the average background wind velocity, V represents the volume of each room, A_w represents the window area. Noted that, the estimated ACH^* of three tests during phase II (BL2, BL3 and BL4) has been adjusted to subtract the ventilation rate caused by the buoyancy effect (ACH_B) summarized in Table 4.

When the room was located windward, the ACH^* value increased with the height of the room getting upward. This indicated that the ventilation rates on the windward side of the street canyon were positively correlated with the height of the room. ACH^* values showed that the ventilation rate of test BW1 was lowest among all of the tests. Note that previous studies [44] investigating the ventilation using CFD simulations in street canyons with an aspect ratio of 1:1 revealed different results: the researchers found that the rooms located on the lowest and highest floors showed the best ventilation performance. This paradox may be attributed to two reasons. First, Ai et al. [44] used an integral method to calculate the ventilation rate by integrating the mean velocities at the opening, while this experiment adopted the tracer gas method. This may cause a difference in the ventilation distributions in the street canyon. Second, in reality, irregular fluctuations of the incoming wind may lead to complex airflow in the street canyon. Steady-state CFD simulations were unable to account for the instant fluctuations near the openings at the middle height of the street canyon and underestimated the ventilation rate.

When the room was located leeward, the variations in the ACH^* values were smaller than those on the windward side. The statistics revealed that the ventilation distribution of the leeward side was more stable than that of the windward side, which indicated that rooms on the windward side of the street canyon may experience stronger perpendicular near-wall airflows than the leeward side.

3.3 Interunit dispersion of building B

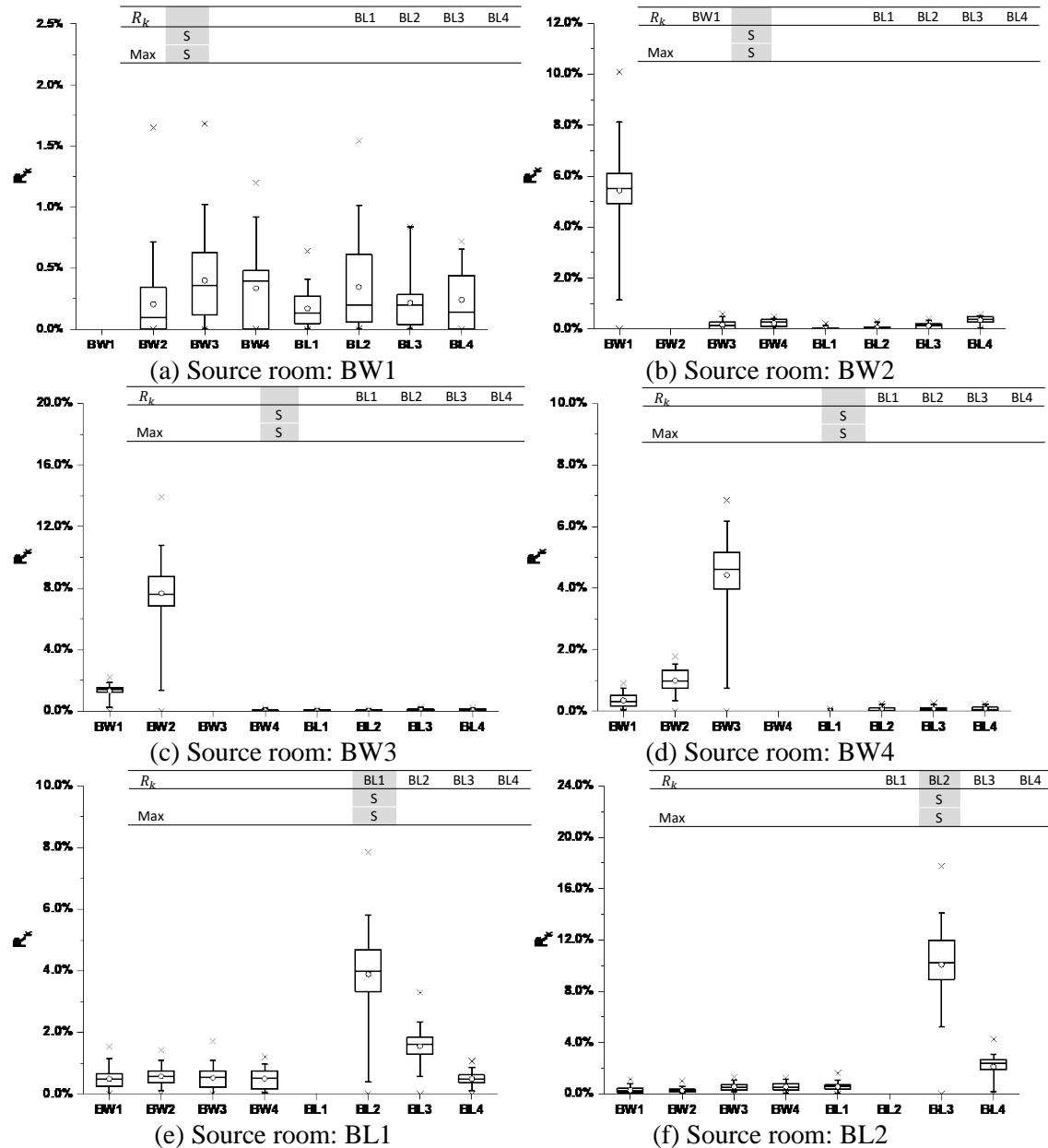
This section describes the analysis of the tracer gas dispersion to each room of building B, based on the data of Round 2 tests from June 9, 2019. Interunit dispersion between the rooms in the same building is dangerous because of the relatively short dispersion distance and time. The reentry ratio was used as an important indicator to assess tracer gas transmissions from the source room to other rooms in the same building. As per equation (4), the term R_k illustrates the fraction of the tracer gas in the source room that reenters another room. Fig. 12 presents box charts of the reentry ratios of each room with respect to different source locations. The mean and maximum values of each test are also listed. The statistical results indicated that the R_k of each room varied significantly based on the source room location, and the reentry ratio in the 1:1 street canyon could reach 17.7% in the test of BL2. Several observations can be made from the comparisons of these tests.

First, when the source was located on the windward side, the reentry ratio of each room was generally lower than that of the leeward side. This may be partly attributed to the fact that the average incoming wind velocities during the windward tests were higher than those of the leeward tests, as presented in the tables in Fig. 10. This accelerated the tracer gas dispersion of the source room and diluted it directly downstream.

Second, the tracer gas was mainly transported downward when the source was located on the windward side, whereas on the leeward side, the tracer gas was mainly transported upward. This phenomenon was caused by the flow characteristics of the 2D street canyon. For an aspect ratio of 1:1 in this experiment, the airflow in the street canyon was termed a skimming flow [45], and a large and stable vortex was formed inside the street canyon. With a strong vortex, the tracer gas transportation routes were established when the source location was fixed. The tracer transportation characteristics in the street canyon had large differences from the conditions of an isolated building [4, 23, 24] or building arrays [25, 26]. Without lateral

separation flows, the tracer gas will disperse from the top of the street canyon or spread horizontally inside the street canyon. Note that in this experiment, only vertical dispersion was considered. The horizontal dispersion of the tracer gas in the street canyon should be analyzed in future studies.

The statistical results of the tests showed that the maximum values of the reentry ratio can be 200% higher than the average values observed in other rooms. Considering $R_k < 1\%$ as a negligible reentry ratio, during the entire Round 2 tests, around 17.9% and 48.2% of rooms were dangerous cases given the average R_k values and maximum R_k values, respectively. This revealed that in a real street-canyon environment, a room has a high probability of occasionally experiencing a high tracer-gas concentration, although the average reentry ratio was very low.



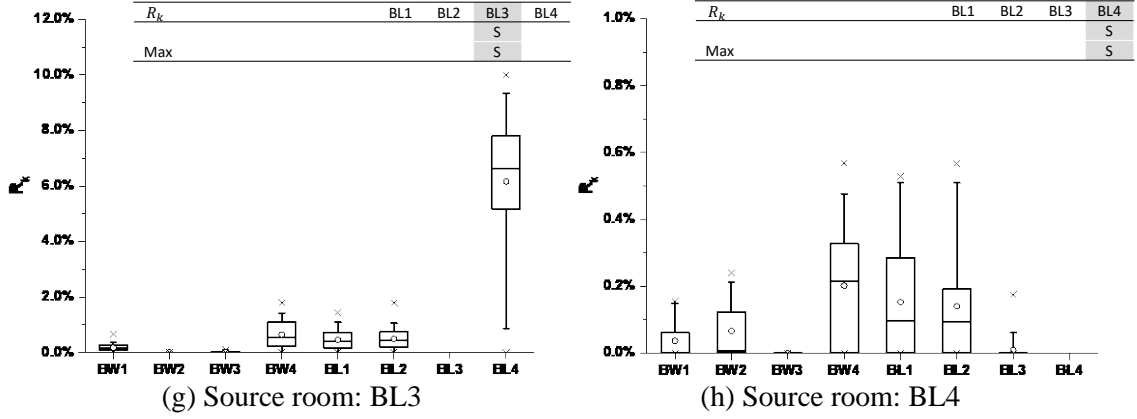


Fig. 12 Box charts of reentry ratio values of each test, with source room marked.

In addition, generally, the highest R_k value as observed room nearest to the source room along the transportation route. Taking source room BL2 as an example, Fig. 13 shows the monitored CO_2 concentrations of the source room and other rooms on the same side during the gas releasing period. It was obvious that the CO_2 concentrations of BL1, BL3, and BL4 were much lower than that of source room BL2. The highest CO_2 concentration occurred in BL3, which was the immediate upper room near BL2. The concentration in room BL3 was around one order lower than that in BL2. The second highest CO_2 concentration was observed in room BL4 at one order lower than that of BL3 and room BL4 located along the vortex path on the leeward side of the street canyon.

The lowest concentration was observed in room BL1. Although this room was very close to the source room, the concentration was three orders lower than that in BL2 as the room was located in the opposite direction of the upward flow along the façade. This phenomenon was also reflected in the value of the average reentry ratio. As shown in Fig. 12(f), the reentry ratio of 10.3% in BL3 decreased to 2.16% in BL4, and the reentry ratio was only 0.53% that of BL1. This further illustrates that the tracer gas was immediately diluted with the upward flow caused by the vortex on the leeward side of the street canyon and merely transported in the reverse direction.

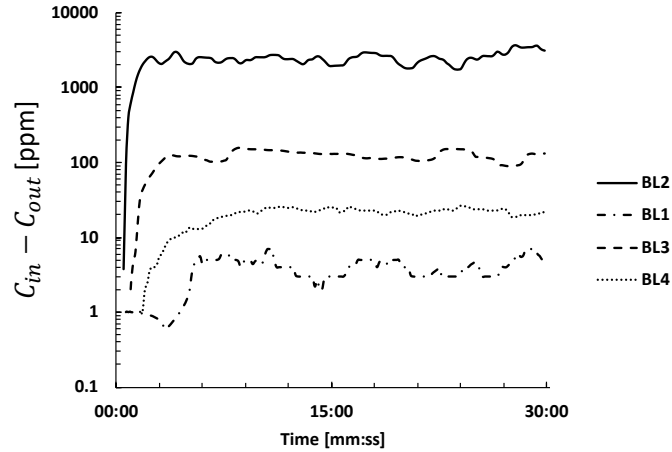


Fig. 13 CO_2 concentration of each source room (BL2) and reentry rooms during gas releasing process for 30 min.

3.4 Comparisons of independent tests for same source location

This section compares three tests conducted at the same source location and under different wind conditions. The source location of room BL2 was selected as an example, because the results of the tracer gas dispersion to other rooms were more straightforward. Table 5 presents the background wind conditions of the three BL2 tests by RainWise automatic

weather station at a height of 2.4 m. \bar{U} represents the average result of the incoming wind velocity in the perpendicular direction to the street canyon (240°), and \bar{U}_{SD} represents the standard deviation of \bar{U} . Tests 1 and 2 were conducted on June 8, 2019, and test 3 was conducted on June 9, 2019. It was observed that during test 2, the wind velocity was significantly lower, and the incoming wind deviated from the normal direction by 43.3° . This value was larger than that observed in tests 1 and 3.

Table 5 Background wind directions and velocities of three BL2 tests.

Test number	Date	Time period	Wind direction [$^\circ$]	Wind velocity [m/s]	\bar{U} [m/s]	\bar{U}_{SD}
1	June 8	10:32–11:02	228.9	3.13	2.95	0.72
2	June 8	21:19–21:49	196.7	1.26	1.05	0.36
3	June 9	15:11–15:41	244.4	2.73	2.50	0.43

Fig. 14 presents the average ventilation rates of source room BL2 and reentry ratios of BL3 and BL4 observed in the three tests with variation in \bar{U} . When the value of \bar{U} increased from 1.05 m/s to 2.50 m/s, the ventilation rate of source room BL2 doubled. However, the ventilation rate no longer increased when \bar{U} was 2.95 m/s. The value of the ventilation rate observed in test 3 was slightly lower than that observed in test 2. This implies that a higher incoming wind velocity does not guarantee a higher ventilation rate in 1:1 street canyons under real weather conditions.

The results for the reentry ratio showed different trends with respect to the ventilation rate. An increasing wind velocity was revealed to suppress the tracer gas dispersion to other rooms. When the incoming wind velocity was as low as 1.05 m/s in the street canyon, the average reentry ratio of BL3 could reach 16.6%, which was quite dangerous. With \bar{U} increased to 2.50 m/s, R_k of BL3 decreased to 10.3% and further decreased to 9.1% when \bar{U} was 2.95 m/s. Similar trends were observed in room BL4. A previous study [14] also showed that a lower wind velocity yielded higher reentry ratios during on-site measurements. In addition, as pointed out in previous research [14, 28] on on-site measurements and CFD simulations, when the incoming wind velocity increased, R_k did not drop further and appeared to be stable. This phenomenon was not obvious in the scaled outdoor experiment owing to the limited number of tests.

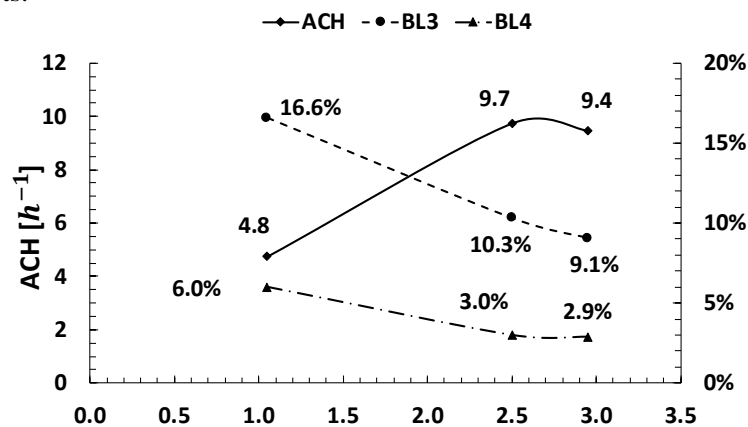


Fig. 14 Average ventilation rates of room BL2 and reentry ratios of rooms BL3 and BL4 with increase in \bar{U} .

3.5 Interunit dispersion to buildings A and C

In this section, the data from June 9, 2019, were acquired to analyze the tracer gas dispersion to rooms of buildings A and C. Table 6 summarizes the maximum reentry ratio of each room in buildings A and C when the source position was located in each room of building B. The reentry ratios equal to or larger than 1% ($R_k > 1\%$) are highlighted. Owing to the longer distance from the source position and more complex airflow movement, the upstream building C and downstream building A suffered lower tracer gas dispersion as compared to the concentration in rooms of building B.

When the source was located on the windward side of building B (BW1 to BW4), the number of highlighted rooms ($R_k > 1\%$) was 15, which is lower than that of the leeward-side source location (BL1 to BL4), which was 21. This may be attributed to the higher average wind velocities of the windward-side tests, which caused the tracer gas to disperse more quickly and shortened the gas residence time in the street canyons. However, although the gas residence time was shorter, the upstream and downstream buildings still experienced high tracer gas concentrations, in particular, in the test with the source room located at BW1.

As presented in Table 6, room AW1 experienced the highest reentry ratio when the source was located in BW1. The maximum reentry ratio reached 3.47% and was larger than those for the rooms in building B, as shown in Fig. 12(a). A similar result occurred in AL1, where the value was 2.91%. This phenomenon was counterintuitive as rooms AW1 and AL1 were at relatively long distances from the source room. This phenomenon further revealed that, in a real street-canyon environment, a room could occasionally experience high tracer-gas concentrations owing to the irregular fluctuations in the street canyon.

Room CL1, located at the opposite position against the street canyon of BW1, also experienced high tracer-gas concentrations in test BW1, where the maximum reentry ratio was 2.52%. The maximum reentry ratios decreased with the increase in building height. This illustrates that the tracer gas released from BW1 was transported partly along the large vortex in the street canyon to the leeward side of building C.

When the sources were located at BW3 and BW4, the tracer gas was directly dispersed from the top of the street canyon and barely entered the next street canyon. Thus, the rooms in buildings A and C suffered negligible reentry ratios.

Conditions with leeward source locations (BL1 to BL4) were more complicated and irregular, not only because of the lower wind velocity during the test period but also partly owing to the varied wind directions. When the sources were located at BL1 and BL2, most of the windward-side rooms of buildings A and C suffered nonnegligible tracer gas concentrations. When the source was located at BL3, the reentry ratios of the leeward-side rooms of buildings A and C were basically nonnegligible.

The conditions of test BL4 were similar to those of BW3 and BW4. The tracer gas was directly dispersed from the top of the street canyon and was rarely transported to other rooms. The irregular tracer-gas dispersion may have occurred because the incoming wind during tests BL1 to BL4 appeared to temporarily reverse direction ($93^\circ - 96^\circ$), although each gust of the reverse incoming wind lasted only 60 s or less. The drastic change in wind direction caused the tracer gas to be transported in multiple directions and spread chaotically.

Table. 6 Maximum reentry ratios of rooms in buildings A and C.

$R_k(\text{Max})$	Source room	BW1	BW2	BW3	BW4	BL1	BL2	BL3	BL4
Downstream	AW1	3.47%	0.67%	0.36%	0.27%	2.37%	0.74%	0.65%	0.12%
	AW2	1.68%	0.32%	0.11%	0.29%	1.06%	1.51%	0.49%	0.14%
	AW3	1.69%	0.14%	0.00%	0.09%	2.17%	3.15%	0.33%	0.57%
	AW4	1.25%	0.65%	0.56%	0.37%	1.43%	1.51%	0.41%	0.17%
	AL1	2.91%	1.14%	0.08%	0.83%	0.16%	1.01%	0.74%	0.51%

	AL2	0.58%	0.31%	0.13%	0.36%	0.38%	0.43%	1.37%	0.20%
	AL3	1.68%	0.56%	0.12%	0.17%	0.52%	0.73%	1.03%	0.14%
	AL4	1.17%	0.82%	0.24%	0.11%	0.67%	0.81%	1.16%	0.28%
Upstream	CW1	2.18%	0.64%	0.20%	0.73%	1.96%	1.61%	0.85%	0.26%
	CW2	0.84%	0.28%	0.12%	0.38%	1.14%	0.75%	0.50%	0.26%
	CW3	2.97%	0.31%	0.13%	0.15%	1.77%	1.35%	0.00%	0.32%
	CW4	1.60%	0.64%	0.41%	0.30%	1.93%	1.98%	0.41%	0.20%
	CL1	2.52%	0.31%	0.81%	0.13%	0.29%	0.55%	1.08%	0.61%
	CL2	1.93%	0.91%	0.14%	0.46%	0.26%	0.37%	1.02%	0.20%
	CL3	1.54%	0.71%	0.00%	0.37%	0.82%	1.32%	0.93%	0.23%
	CL4	1.23%	0.64%	0.49%	0.15%	0.11%	0.09%	0.91%	0.61%

4. Limitations

The results of this study were based on weather conditions of the summer season (June) in a suburban area of Guangzhou, which is a humid subtropical climate region. During the test period, the majority of the wind velocities varied from 1.0–5.0 *m/s*, and the frequency was higher than 80%. Low wind conditions (lower than 1.0 *m/s*) and high wind conditions (higher than 5.0 *m/s*) were not captured by this experiment. Especially for the low wind conditions, when the incoming wind was less than 1.0 *m/s*, the wind velocity in the street canyon was even lower. With a temperature difference between the indoor and outdoor air, the driving force could become complicated and lead to different results for the ventilation rate and tracer gas dispersion. Since this paper mainly analyzes the wind effect, the characteristics of the ventilation performance and tracer gas dispersion in the street canyon with the combined buoyancy and wind effect need further investigation.

Then, owing to restrictions on the room volume, only one CO_2 sensor was set in each room to monitor the tracer gas concentration. Without a mechanical driving force and owing to its dispersal by pure wind, the uniformity of the tracer gas concentration in each room was difficult to ensure. The ACH and reentry ratio equations (3) and (4) were calculated based on well-mixed indoor tracer gas, which may lead to inaccuracies in the ventilation and reentry-ratio results.

In addition, this study considered only single-sided ventilation and a typical shape of window (rectangular shape and the window to wall ratio is 0.13), but real buildings have different numbers and shapes of windows. All these factors could influence the results of ventilation rate and pollutant dispersion described in this paper, and this will be explored in our future studies.

5. Conclusions

This study conducted a scaled outdoor experiment to explore the interunit dispersion problem in a 2D street canyon with the tracer gas method. A series of measurements were performed to investigate the ventilation performance and interunit dispersion. The ventilation rates of the source room were acquired by CO_2 constant release, and the interunit tracer gas transmission was quantified by the reentry ratio. The conclusions can be drawn as follows:

- (1) Based on the weather conditions of the test day, the ventilation performance of the source rooms varied with the room location. The ventilation distribution of the leeward-side room was more stable than that of the windward side.
- (2) The interunit dispersion between rooms in the source building changed significantly with the source room location. Owing to a large and stable vortex constructed by the freestream inside the street canyon, the tracer gas was mainly transported in the vortex direction, and the

highest R_k value occurred generally in the room nearest to the source room along the transportation route.

(3) The general interunit dispersion between rooms in separate buildings was much smaller than that in the source building. However, owing to highly fluctuating wind conditions, rooms located in separate buildings may occasionally have larger reentry ratios than rooms located in the source building.

Acknowledgement

This work was supported by a PhD studentship funded by Hong Kong Polytechnic University. The experiment described in this paper was conducted at Sun Yat-sen University. It is declared that all authors do not have a conflict of interest. This study was financially supported by National Natural Science Foundation--Outstanding Youth Foundation(No. 41622502), STINT(dnr CH2017-7271) and the National Natural Science Foundation of China(No.51811530017 and 41875015)

References:

1. J. Robinson, and W. Nelson, National human activity pattern survey data base. USEPA, Research Triangle Park, NC, 1995.
2. N.E. Klepeis, W.C. Nelson, W.R. Ott, J.P. Robinson, A.M. Tsang, P. Switzer, J.V. Behar, S.C. Hern and W.H. Engelmann, The National Human Activity Pattern Survey (NHAPS): a resource for assessing exposure to environmental pollutants. *Journal of Exposure Science and Environmental Epidemiology*, 2001. 11(3): p. 231.
3. A. Handbook, ASHRAE Handbook--Fundamentals. Atlanta, GA, 2009.
4. Z.T. Ai, Numerical investigation of single-sided natural ventilation and interunit dispersion in multistory buildings. 2015, The Hong Kong Polytechnic University.
5. R.Z. Homod and K.S.M. Sahari, Energy savings by smart utilization of mechanical and natural ventilation for hybrid residential building model in passive climate. *Energy and Buildings*, 2013. 60: p. 310-329.
6. T. Schulze and U. Eicker, Controlled natural ventilation for energy efficient buildings. *Energy and Buildings*, 2013. 56: p. 221-232.
7. Y. Tominaga and T. Stathopoulos, Ten questions concerning modeling of near-field pollutant dispersion in the built environment. *Building and Environment*, 2016. 105: p. 390-402.
8. S.J. Cao and J. Meyers, On the construction and use of linear low - dimensional ventilation models. *Indoor Air*, 2012. 22(5): p. 427-441.
9. J.M. Santos, I. Mavroidis, N.C. Reis Jr, and E.C. Pagel, Experimental investigation of outdoor and indoor mean concentrations and concentration fluctuations of pollutants. *Atmospheric Environment*, 2011. 45(36): p. 6534-6545.
10. Z.T. Ai, C.M. Mak, and J.L. Niu, Numerical investigation of wind - induced airflow and interunit dispersion characteristics in multistory residential buildings. *Indoor air*, 2013. 23(5): p. 417-429.
11. I.T. Yu, Y. Li, T.W. Wong, W. Tam, A.T. Chan, J.H. Lee, D.Y. Leung and T. Ho, Evidence of airborne transmission of the severe acute respiratory syndrome virus. *New England Journal of Medicine*, 2004. 350(17): p. 1731-1739.
12. Y. Li, S. Duan, I.T. Yu and T.W. Wong, Multi - zone modeling of probable SARS virus transmission by airflow between flats in Block E, Amoy Gardens. *Indoor air*, 2005. 15(2): p. 96-111.
13. J. Mao and N.P. Gao, The airborne transmission of infection between flats in high-rise residential buildings: A review. *Building and Environment*, 2015. 94: p. 516-531.
14. J.L. Niu, and T. Tung, On - site quantification of re - entry ratio of ventilation exhausts in multi - family residential buildings and implications. *Indoor Air*, 2008. 18(1): p. 12-26.

15. N.P. Gao, J.L. Niu, M. Perino and P. Heiselberg, The airborne transmission of infection between flats in high-rise residential buildings: Particle simulation. *Building and Environment*, 2009. 44(2): p. 402-410.
16. J.H. Wang, J.L. Niu, X.P. Liu and C.W.F. Yu, Assessment of pollutant dispersion in the re-entrance space of a high-rise residential building, using wind tunnel simulations. *Indoor and Built Environment*, 2010. 19(6): p. 638-647.
17. D. Mu, N.P. Gao, and T. Zhu, Wind tunnel tests of inter-flat pollutant transmission characteristics in a rectangular multi-storey residential building, part A: Effect of wind direction. *Building and Environment*, 2016. 108: p. 159-170.
18. D. Mu, C. Shu, N.P. Gao and T. Zhu, Wind tunnel tests of inter-flat pollutant transmission characteristics in a rectangular multi-storey residential building, part B: Effect of source location. *Building and Environment*, 2017. 114: p. 281-292.
19. X.P. Liu, J.L. Niu, K.C. Kwok, J.H. Wang and B.Z. Li, Investigation of indoor air pollutant dispersion and cross-contamination around a typical high-rise residential building: Wind tunnel tests. *Building and Environment*, 2010. 45(8): p. 1769-1778.
20. L. Li and C.M. Mak, The assessment of the performance of a windcatcher system using computational fluid dynamics. *Building and environment*, 2007. 42(3): p. 1135-1141.
21. X.P. Liu, J.L. Niu, M. Perino and P. Heiselberg, Numerical simulation of inter-flat air cross-contamination under the condition of single-sided natural ventilation. *Journal of Building Performance Simulation*, 2008. 1(2): p. 133-147.
22. N.P. Gao, J.L. Niu, M. Perino and P. Heiselberg, The airborne transmission of infection between flats in high-rise residential buildings: Tracer gas simulation. *Building and Environment*, 2008. 43(11): p. 1805-1817.
23. Z.T. Ai and C.M. Mak, A study of interunit dispersion around multistory buildings with single-sided ventilation under different wind directions. *Atmospheric Environment*, 2014. 88: p. 1-13.
24. Z.T. Ai and C.M. Mak, Large eddy simulation of wind - induced interunit dispersion around multistory buildings. *Indoor air*, 2016. 26(2): p. 259-273.
25. D.J. Cui, C.M. Mak, K.C.S. Kwok, Z.T. Ai CFD simulation of the effect of an upstream building on the inter-unit dispersion in a multi-story building in two wind directions. *Journal of Wind Engineering and Industrial Aerodynamics*, 2016. 150: p. 31-41.
26. Y.W. Dai, C.M. Mak, Z.T. Ai Computational fluid dynamics simulation of wind-driven inter-unit dispersion around multi-storey buildings: Upstream building effect. *Indoor and Built Environment*, 2019. 28(2): p. 217-234.
27. D. Mu, N.P. Gao, and T. Zhu, CFD investigation on the effects of wind and thermal wall-flow on pollutant transmission in a high-rise building. *Building and Environment*, 2018. 137: p. 185-197.
28. Y.W. Dai, C.M. Mak, Z.T. Flow and dispersion in coupled outdoor and indoor environments: Issue of Reynolds number independence. *Building and Environment*, 2019. 150: p. 119-134.
29. E. Yee and C.A. Biltoft, Concentration fluctuation measurements in a plume dispersing through a regular array of obstacles. *Boundary-Layer Meteorology*, 2004. 111(3): p. 363-415.
30. A. Dallman, S. Magnusson, R. Britter, L. Norford, D. Entekhabi and H.J.S. Fernando, Conditions for thermal circulation in urban street canyons. *Building and Environment*, 2014. 80: p. 184-191.
31. S. Onomura, H. Takimoto and M. Kanda. Influence of a heated wall on urban canopy flow using PIV measurements. in *Seventh International Conference on Urban Climate (ICUC)*, Yokohama, Japan. 2009.
32. T. Kawai and M. Kanda, Urban energy balance obtained from the comprehensive outdoor scale model experiment. Part I: Basic features of the surface energy balance. *Journal of Applied Meteorology and Climatology*, 2010. 49(7): p. 1341-1359.
33. A. Nottrott, S. Onomura, A. Inagaki, M. Kanda and J. Kleissl, Convective heat transfer on leeward building walls in an urban environment: measurements in an outdoor scale model. *International Journal of Heat and Mass Transfer*, 2011. 54(15-16): p. 3128-3138.

34. M. Park, A. Hagishima, J. Tanimoto and K. Narita, Effect of urban vegetation on outdoor thermal environment: field measurement at a scale model site. *Building and Environment*, 2012. 56: p. 38-46.
35. N.I. Syafii, M. Ichinose, E. Kumakura, S.K. Jusuf, K. Chigusa and N.H. Wong, Thermal environment assessment around bodies of water in urban canyons: A scale model study. *Sustainable Cities and Society*, 2017. 34: p. 79-89.
36. X.X. Li, D.Y.C. Leung and C.H. Liu, Physical modeling of flow field inside urban street canyons. *Journal of Applied Meteorology and Climatology*, 2008. 47(7): p. 2058-2067.
37. Z.T. Ai, C.M. Mak, D.J. Cui and P. Xue, Ventilation of air-conditioned residential buildings: A case study in Hong Kong. *Energy and Buildings*, 2016. 127: p. 116-127.
38. Y. Wu, T.C. Tung, and J.L. Niu, On-site measurement of tracer gas transmission between horizontal adjacent flats in residential building and cross-infection risk assessment. *Building and Environment*, 2016. 99: p. 13-21.
39. Z.T. Ai and C.M. Mak, CFD simulation of flow in a long street canyon under a perpendicular wind direction: Evaluation of three computational settings. *Building and Environment*, 2017. 114: p. 293-306.
40. E.S. So, A.T. Chan, and A.Y. Wong, Large-eddy simulations of wind flow and pollutant dispersion in a street canyon. *Atmospheric environment*, 2005. 39(20): p. 3573-3582.
41. P. Bradshaw, The analogy between streamline curvature and buoyancy in turbulent shear flow. *Journal of Fluid Mechanics*, 1969. 36(1), pp.177-191.
42. A. Walker, Natural ventilation. National Renewable Energy Laboratory (US Department of Energy), 2014.
43. G. Lane-Serff, Heat flow and air movement in buildings. 1989, University of Cambridge.
44. Z.T. Ai and C.M. Mak, Wind-induced single-sided natural ventilation in buildings near a long street canyon: CFD evaluation of street configuration and envelope design. *Journal of Wind Engineering and Industrial Aerodynamics*, 2018. 172: p. 96-106.
45. T. Oke, Boundary layer climates, 372. Methuen, New York, 1978.